*The Company of* **Biologists**

# RESEARCH ARTICLE

# Platelet-derived microvesicles regulate vascular smooth muscle cell energy metabolism via PRKAA after intimal injury

Jing Yan[1],*, Yang-Jing Fan[1],*, Han Bao[1], Yong-Guang Li[2], Shou-Min Zhang[1], Qing-Ping Yao[1], Yun-Long Huo[1], Zong-Lai Jiang[1], Ying-Xin Qi[1] and Yue Han[1],‡

## ABSTRACT

Vascular intimal injury initiates various cardiovascular disease processes. Exposure to subendothelial collagen can cause platelet activation, leading to collagen-activated platelet-derived microvesicles (aPMVs) secretion. In addition, vascular smooth muscle cells (VSMCs) exposed to large amounts of aPMVs undergo abnormal energy metabolism; they proliferate excessively and migrate after the loss of endothelium, eventually contributing to neointimal hyperplasia. However, the roles of aPMVs in VSMC energy metabolism are still unknown. Our carotid artery intimal injury model indicated that platelets adhered to injured blood vessels. *In vitro*, phosphorylated Pka (cAMP-dependent protein kinase) content was increased in aPMVs. We also found that aPMVs significantly reduced VSMC glycolysis and increased oxidative phosphorylation, and promoted VSMC migration and proliferation by upregulating phosphorylated PRKAA (α catalytic subunit of AMP-activated protein kinase) and phosphorylated FoxO1. Compound C, an inhibitor of PRKAA, effectively reversed the enhancement of cellular function and energy metabolism triggered by aPMVs *in vitro* and neointimal formation *in vivo*. We show that aPMVs can affect VSMC energy metabolism through the Pka-PRKAA-FoxO1 signaling pathway and this ultimately affects VSMC function, indicating that the shift in VSMC metabolic phenotype by aPMVs can be considered a potential target for the inhibition of hyperplasia. This provides a new perspective for regulating the abnormal activity of VSMCs after injury.

KEY WORDS: Intimal injury, Platelet-derived microvesicles, Cell energy metabolism, Vascular smooth muscle cells, PRKAA

## INTRODUCTION

Vascular intimal injury initiates the progression of cardiovascular diseases (CVDs), such as vascular restenosis and atherosclerosis (Carracedo et al., 2019; Tesfamariam, 2016). Hence, it is necessary to inhibit neointimal thickening and accelerate reendothelialization after vascular intimal damage. Vascular smooth muscle cells (VSMCs) are the main component of the media vasculature, and their migration (Cheong et al., 2011) and proliferation (Merlet et al., 2013) have been found to be important factors that regulate the thickening of the vascular wall and narrowing of the vascular lumen after vascular intimal injury. The migration of VSMCs from the tunica media to the intima plays a key role in the vascular remodeling process, and the inhibition of VSMC migration into the intimal layer in response to arterial wall injury can effectively decrease neointimal hyperplasia (Zhuang et al., 2019).

Subendothelial collagen is exposed after intimal damage, and platelets are recruited and attach to the site of injury (Seifert et al., 2017). The adhered platelets are then activated by collagen and consequently produce massive platelet-derived microvesicles (PMVs) (Boilard et al., 2010). Increasing numbers of reports suggest that platelet microvesicles are involved in the process of CVDs, such as atherosclerosis (Rosińska et al., 2017). They participate in regulating recipient cell function by transferring platelet-derived cargos, such as proteins and microRNAs. Exposing VSMCs to platelet-derived growth factor-BB homodimer (PDGF-BB) results in mitochondrial fragmentation and VSMC phenotypic changes, which are accompanied by changes in energy metabolism processes (Salabei and Hill, 2013). However, the effect of platelets and derived microvesicles on VSMC energy metabolism after vascular injury is still unclear.

Glycolysis and mitochondrial oxidative phosphorylation (OXPHOS) are the two main pathways involved in cell energy metabolism. Glycolysis is a universal metabolic process in living cells, and cells use glycolysis to produce energy under hypoxic conditions (Rigoulet et al., 2020). Both mitochondrial respiration and glycolysis play crucial roles in the cell growth and development. Perez et al. (2010) found that mitochondrial respiration and glycolysis are enhanced in response to PDGF, which is consistent with PDGF-induced VSMC proliferation. Mitochondria are the energy factories of cells and are closely related to the energy metabolism state in most cell types (Wanet et al., 2015). In addition, mitochondria are also the main sites of oxidative metabolism in eukaryotes. Under normal conditions, cells use glucose to produce most of the required ATP through mitochondrial OXPHOS (Zeng et al., 2020).

It is important to identify the key molecules that drive VSMC migration and metabolism and develop targeted therapies aimed at these key molecules. AMP-activated protein kinase (AMPK) is an energy regulator that is present in a complex network of metabolic signaling pathways (Faubert et al., 2015), and it is a promising therapeutic target for type II diabetes, cancer and other diseases characterized by the abnormal utilization of energy (Sinnetta and Brenman, 2014). In different species, AMPK is present as a heterotrimeric complex that consists of an α catalytic subunit (PRKAA), a β regulatory subunit and a γ regulatory subunit. AMPK can regulate intracellular energy homeostasis via glucose and lipid metabolism and also participates in many cell functions. Previous studies have shown that AMPK is considered a key factor in the regulation of VSMC function. For example, AMPK was found to be involved in inhibiting VSMC proliferation induced by PDGF by pioglitazone (Osman and Segar, 2016). Zhang et al. (2019)

[1]Institute of Mechanobiology & Medical Engineering, School of Life Sciences & Biotechnology, Shanghai Jiao Tong University, Shanghai 200240, China. [2]Department of Cardiology, Shanghai Jiao Tong University Affiliated Sixth People's Hospital, Shanghai 200233, China.
*These authors contributed equally to this work

‡Author for correspondence (hanyue625@sjtu.edu.cn)

Y.H., 0000-0002-1362-4897

demonstrated that the AMPK-Nox4 signaling pathway is involved in the protective effects of metformin and linagliptin against neointimal hyperplasia of the carotid artery after balloon injury in diabetic rats, and it functions by inhibiting VSMC remodeling.

In this study, we established a carotid artery injury model in Sprague-Dawley (SD) rats and observed the adhesion of platelets to VSMCs at the injury site. The role of collagen-activated platelet-derived microvesicles (aPMVs) in regulating VSMC energy metabolism and cell function after intimal injury was explored, and we also investigated the molecular mechanism involved in the process. The aim of our study was to discover how aPMVs regulate VSMC energy metabolism and identify a therapeutic target for the inhibition of excessive hyperplasia.

## RESULTS

### Platelets adhere to the intimal injury site *in vivo*

To investigate the role of VSMCs in vascular remodeling, we established a carotid artery balloon intimal injury model in rats

(Fig. 1A). The left common carotid artery of the rat was used as the experimental group and the right common carotid artery was considered the autologous control group. Two weeks after the injury, we observed clear intimal hyperplasia of the injured left carotid artery using Hematoxylin-Eosin staining. The area of the vascular media showed no change (Fig. S1), but a significant increase in the vascular wall area (media and neointima) and a decrease in the lumen area were detected in the injured vessels, indicating a thickening of the neointima (Fig. 1B). In addition, 1 h after the surgery, common carotid arteries were harvested, and the von Willebrand factor (vWF), a specific marker of endothelial cells (ECs), was not expressed in the damaged left carotid artery but present in the intact right carotid artery. The loss of the vWF fluorescence indicated that the intimal injury model was successfully established (Fig. 1C). In addition, staining for α-smooth muscle actin (α-SMA) and the platelet marker CD41 showed that platelets adhered to the intimal injury site of the left common carotid artery 1 h after intimal injury, but there was no
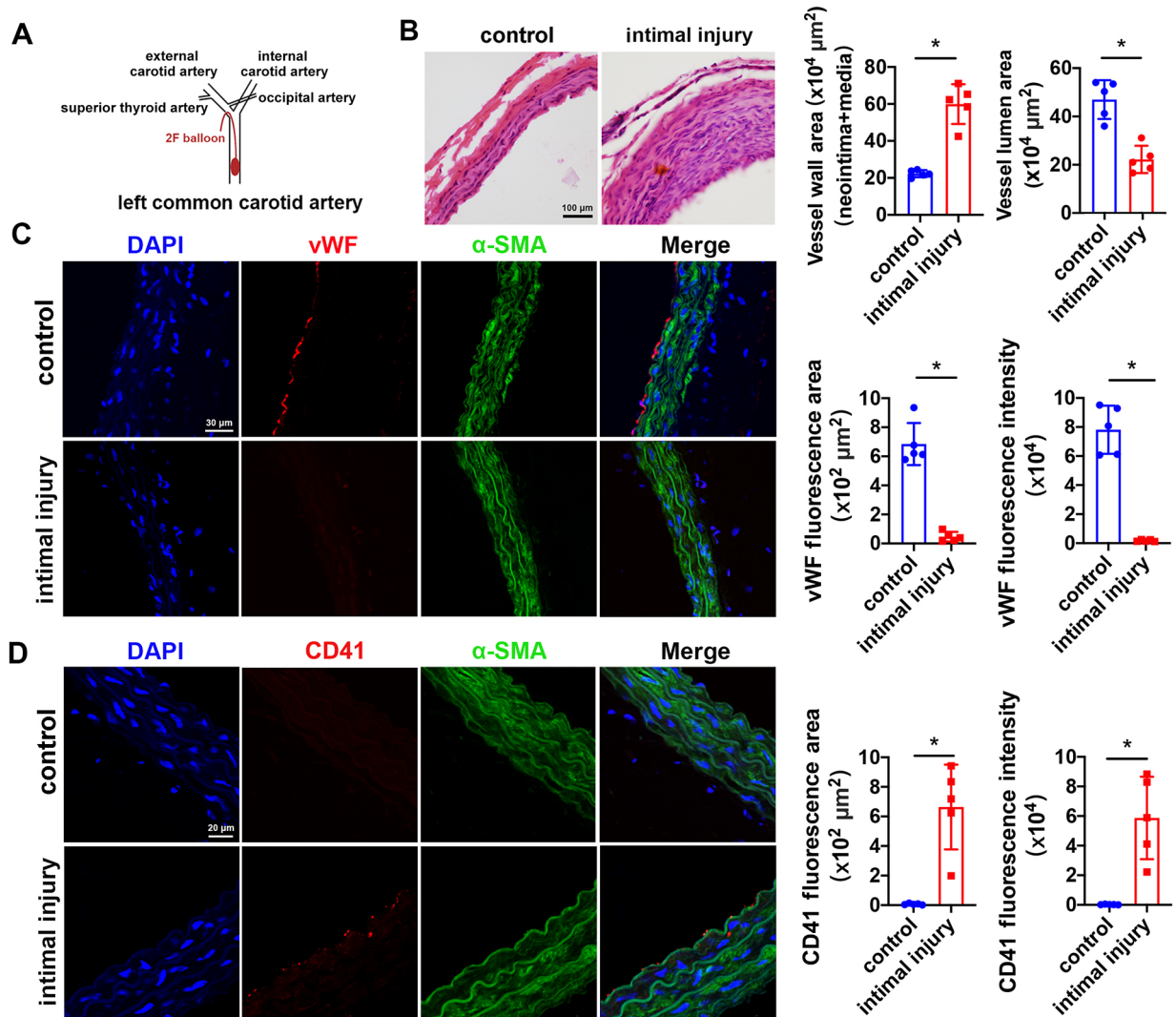


Fig. 1. Adhesion of platelets in the rat intimal injury model. (A) Schematic diagram showing the establishment of the Sprague-Dawley (SD) rat intimal injury model. (B) Hematoxylin-Eosin (HE) staining revealed significant intimal hyperplasia in the intimal injury group 2 weeks after surgery compared with the control group. ImageJ was used to quantify the vessel wall area and lumen area (*n*=5 animals). Scale bar: 100 μm. (C) Endothelial denudation was observed at 1 h after surgery by *in situ* immunofluorescence staining for DAPI (blue), vWF (red, a specific marker of endothelium), and α-SMA (green). The vWF fluorescence area and intensity were significantly decreased after intimal injury (*n*=5 animals). Scale bar: 30 μm. (D) Immunofluorescence staining was used to explore the adhesion of platelets to VSMCs at 1 h after surgery. CD41 is a specific marker of platelets marked in red, and the fluorescence area and intensity were increased compared with those of the control (*n*=5 animals). Scale bar: 20 μm. *P*-value was calculated by two-tailed Mann–Whitney test (B–D). The values are the mean±s.d. *$P<0.05$.

CD41 expression in the right common carotid artery (Fig. 1D). All the *in vivo* findings indicated that the surgery caused endothelial denudation and platelets adhered to the injury site. Aggregated platelets can be activated by exposed collagen after injury and form a local microenvironment. An important way for platelets to function is by releasing microvesicles. Hence, we hypothesized that collagen-activated platelet-derived microvesicles (aPMVs) might participate in VSMC signaling pathway regulation.

## aPMVs promote VSMC migration

VSMCs were isolated from the thoracic aortas of Sprague-Dawley (SD) rats. To explore the effect of aPMVs on VSMCs *in vitro*, platelets were obtained from the abdominal aorta blood of SD rats and activated by incubating them with or without collagen (1 μl/ml) for 1 h. Then microvesicles were obtained by centrifugation at 20,500 *g* for 90 min, as described in the schematic diagram (Fig. 2A). To identify microvesicles derived from platelets,
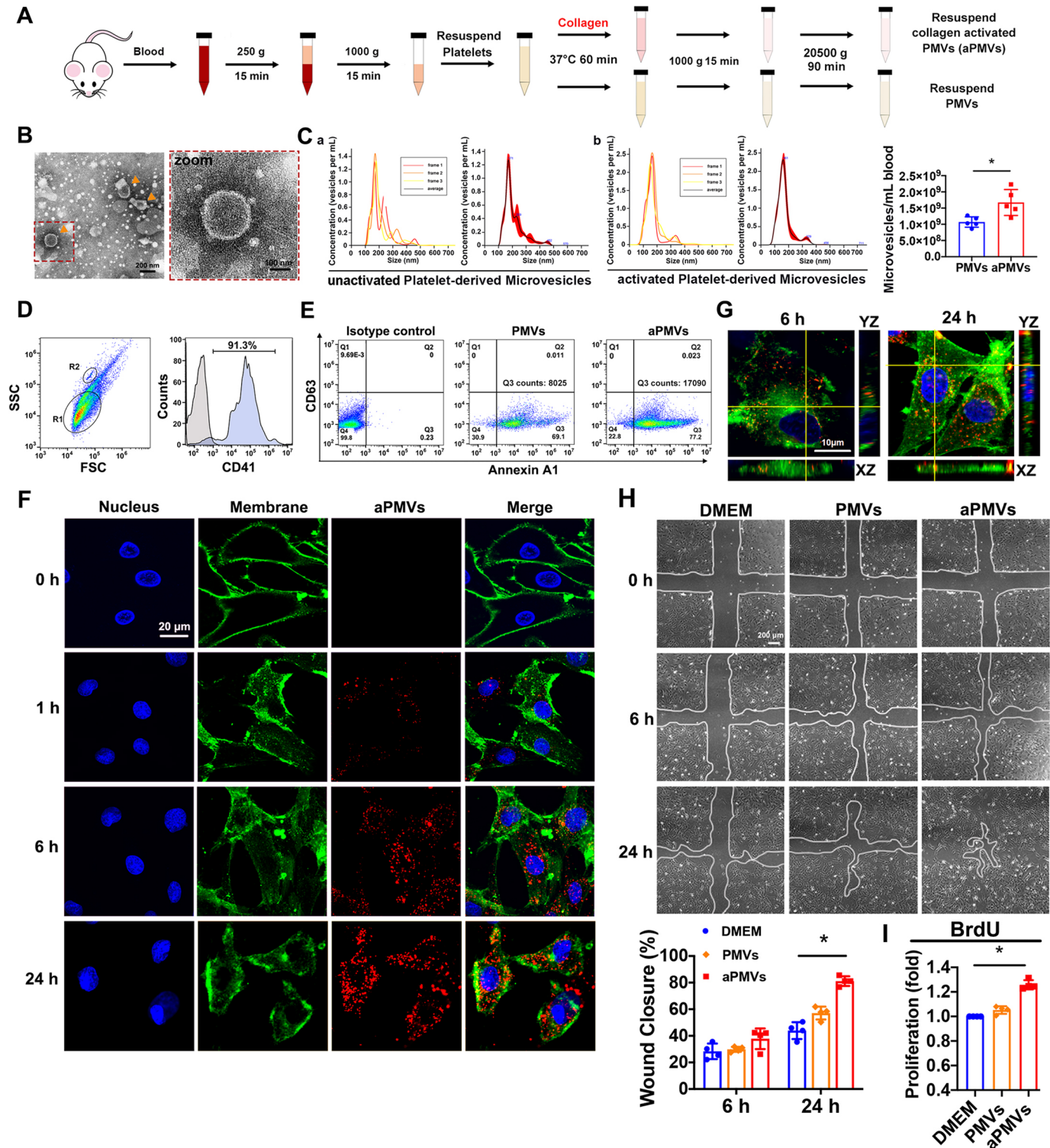


**Fig. 2.** See next page for legend.

**Fig. 2. Treatment with aPMVs significantly accelerates the migration and proliferation of VSMCs.** (A) Flow diagram of the method used to collect microvesicles. (B) TEM was used to visualize the aPMVs (indicated by arrowheads). Scale bars: 200 nm and 100 nm. (C) NTA was used to detect the concentration and size of the collected PMVs. The left panels in a,b represent three replicates from one sample test, and the right panels represent the average. The results indicated that the size of most PMVs was between 100 and 300 nm (a,b) and that the concentration of activated PMVs was increased compared with that of unactivated PMVs (right) ($n$=5). (D) aPMVs (gate R1) were defined by 2.5–4.5 μm beads (gate R2) (left). FACS analysis showed that over 90% of the microvesicles were CD41 positive (right). FSC, forward scatter; SSC, side scatter. (E) PMVs and aPMVs were defined as CD63⁻/Annexin A1⁺ events in the Q3 window and they were used for quantification. The aPMVs counts were significantly higher than those of PMVs. (F) aPMVs significantly adhered to the VSMC membrane after 1 h of incubation and adhesion increased with the prolonged incubation time. aPMVs were labeled in red with PKH26, and VSMC membranes were labeled in green with DiO live cell membrane fluorescent probe. Hoechst 33342-stained nuclei in blue. Scale bar: 20 μm. (G) The z-axis images taken at 6 h and 24 h showed that aPMVs had been endocytosed into cells. Scale bar: 10 μm. (H) Wound healing assay showed that VSMC migration was significantly increased after 24 h of incubation with aPMVs ($n$=4 independent experiments). Scale bar: 200 μm. (I) The BrdU assay showed that VSMC proliferation was significantly upregulated after 24 h of incubation with aPMVs ($n$=4 independent experiments). $P$-value was calculated by two-tailed Mann–Whitney test (C) and Kruskal–Wallis test with uncorrected Dunn's test (H,I). The values are the mean±s.d. *$P$<0.05.

transmission electron microscopy (TEM), nanoparticle tracking analysis (NTA) and flow cytometry were used in accordance with the Minimal Information for Studies of Extracellular Vesicles (MISEV) 2018 guidelines, which were proposed by The International Society for Extracellular Vesicles (ISEV) (Théry et al., 2018). As shown in Fig. 2B, the vesicles were approximately 200 nm in size and had a clear, intact spherical structure. The size range of the microvesicles was further quantified by NTA, and collagen activation significantly increased the concentration of aPMVs (Fig. 2C). The flow cytometry results indicated that microvesicles (gate R1) were defined with 2.5–4.5 μm beads (gate R2), and high expression of the platelet marker CD41 (>90%) (Fig. 2D). The exosome marker CD63 (Mathieu et al., 2021) and the microvesicle marker Annexin A1 (Jeppesen et al., 2019) were used to identify aPMVs, which were Annexin A1-positive and CD63-negative (Fig. 2E). Then, the adhesion of aPMVs to VSMCs was detected *in vitro*.

The results showed that aPMVs that were positive for PKH26, a fluorescent dye that stably stains live-cell membranes in bright red, adhered to the VSMC membrane after 1 h of incubation and that adhesion increased with longer incubation times (Fig. 2F). Moreover, the z-axis images taken at 6 h and 24 h showed that aPMVs had been endocytosed into cells (Fig. 2G). The migration of VSMCs to the intima at the vascular injury site is a key factor in the development of intimal hyperplasia. Wound healing assays demonstrated that aPMV treatment significantly enhanced the migration of VSMCs at 24 h, which was not significantly modified by Dulbecco's Modified Eagle Medium (DMEM, negative control) or PMV treatment, the latter of which gave results similar to cells in the normal physiological state (Fig. 2H). The BrdU assay suggested an upregulated proliferation level of VSMCs under aPMV stimulation (Fig. 2I). Compared with aPMV treatment, PMV treatment did not significantly regulate VSMC function. This finding might be caused by the activation of collagen, which allows platelets to release specific types of microvesicles selectively. Therefore, we next investigated the effect of aPMVs on VSMC function.

## aPMVs alter the VSMC energy metabolic profile

Increased cell migration and proliferation are closely related to energy metabolism. Mitochondria are the main organelles that produce ATP, and the local ATP concentration directly regulates cellular motility, so the mitochondrial subcellular distribution is often associated with the energetic states of cells. To explore whether aPMVs altered VSMC energy metabolism, mitochondria were first detected by fluorescence staining with MitoTracker Red. The mitochondria in the VSMCs were concentrated around the nucleus in the DMEM control group, while they tended to be distributed in the cytoplasm after stimulation with aPMVs (Fig. 3A). Using the center of each nucleus as the coordinate origin, quantification of mitochondrial distribution analyzed by CellSens software showed that the average distance of mitochondria from the center was significantly increased after stimulation with aPMVs (Fig. 3B). Additionally, aPMV treatment caused the mitochondria to be distributed farther from the center of the cell, compared with the DMEM control group (Fig. 3C).

In addition to their wide cellular distribution, mitochondria are highly dynamic and can undergo fusion, fission, transport and degradation, which are involved in the regulation of bioenergetics (Mishra and Chan, 2016). Changes in VSMC mitochondrial distribution might also contribute to shifts in the cellular energy phenotype. To detect the energy metabolic state of VSMCs, we first measured the oxygen consumption rate (OCR), which represents the OXPHOS activity in VSMCs (Fig. 3D). Treatment with aPMVs significantly enhanced the mitochondrial respiration capacity of the VSMCs, including basal OCR (Fig. 3E), maximum mitochondrial respiration (Fig. 3F) and ATP production (Fig. 3G). Next, we analyzed the extracellular acidification rate (ECAR), which indicates the glycolytic level of VSMCs (Fig. 3H). Following the addition of glucose, oligomycin and the glycolysis inhibitor 2-deoxy-D-glucose (2-DG) in sequence, VSMC glycolysis levels (Fig. 3I), glycolytic capacity (Fig. 3J) and glycolytic reserve (Fig. 3K), respectively, were detected. The results showed that aPMV addition reduced the level of cellular ECAR. Seahorse extracellular flux analyses suggested that the stimulation of aPMVs shifted the VSMC energy phenotype, causing aerobic respiration to provide more energy than glycolysis (Fig. 3L). In summary, aPMVs regulated the metabolic profile of VSMCs. Increased mitochondrial respiration provided energy for the proliferation of VSMCs, while dispersed mitochondria were more conducive to cell migration.

## aPMVs regulate p-PRKAA and NAD⁺ through p-Pka

AMPK is a critical regulator of mitochondrial biogenesis, and thus, we detected the activation of its α-catalytic subunit PRKAA via phosphorylation at Thr172. aPMV treatment significantly increased the levels of phosphorylated PRKAA (p-PRKAA) after 1 h of incubation. However, the activation effect did not persist and was significantly reduced at 6 h and 24 h (Fig. 4A). The significant decrease in p-PRKAA might be due to its involvement in the activation of downstream molecules. NAD⁺ is regarded as an important coenzyme in metabolic processes. Cantó et al. (2009) showed that PRKAA activation can significantly increase the content of downstream NAD⁺. The results of the Ingenuity pathway analysis (IPA) also revealed a direct relationship between AMPK and NAD⁺ (Fig. S2). The content and ratio of NAD⁺/NADH were not significantly altered following aPMV treatment after 1 h (Fig. 4B,C). However, the NAD⁺ and NADH content increased significantly 6 h and 24 h after aPMV stimulation, in response to the activation of p-PRKAA (Fig. 4D–G). The results demonstrated that
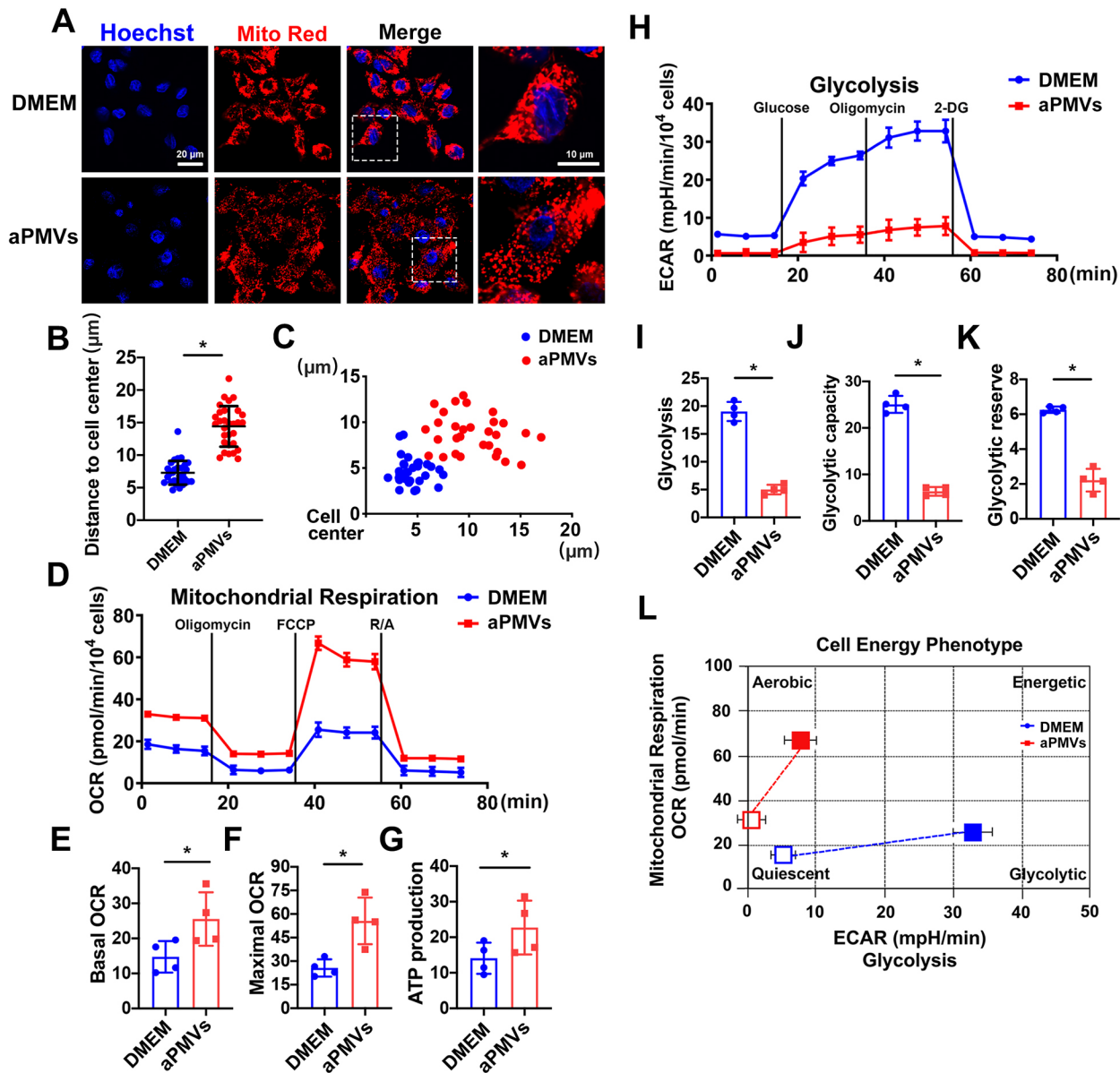
**Fig. 3. aPMVs change the mitochondrial distribution and energy metabolic profile of VSMCs.** (A) Effect of aPMVs on the mitochondrial distribution in VSMCs. Cells were stained with MitoTracker Red (Mito Red) and Hoechst 33342 for 30 min at 37°C. Scale bars: 20 µm and 10 µm. (B,C) The average distance (B) and average coordinates (C) of mitochondria from the cell center were analyzed with CellSens software ($n$=30 independent cells). (D) Representative traces of the oxygen consumption rate (OCR) in VSMCs with or without aPMV incubation. (E) Basal OCR, (F) maximal OCR and (G) ATP production were measured and compared (D–G, $n$=4 independent experiments). (H) Representative traces of the extracellular acidification rate (ECAR) in VSMCs with or without aPMV incubation. (I–K) Measurement of (I) glycolysis, (J) glycolytic capacity and (K) glycolytic reserve in VSMCs (H–K, $n$=4 independent experiments). (L) Calculation of the energy phenotype in VSMCs. The empty squares represent the basal cell states, and the filled squares represent the stressed cell states ($n$=4 independent experiments). $P$-values were calculated by unpaired two-tailed Student's $t$-test (B) and two-tailed Mann–Whitney test (E–G,I–K). The values are the mean±s.d. *$P$<0.05. mpH, milli pH units.

the p-PRKAA-NAD$^+$ pathway was involved in the energy metabolism of VSMCs regulated by aPMVs.

To explore the mechanisms by which aPMVs regulated the phosphorylation of PRKAA, we used IPA to analyze the upstream regulators of PRKAA. A total of 123 upstream molecules of PRKAA were found and were divided into four categories based on their location in the cell (Fig. 4H). In addition, Milioli et al. reported the protein profiles of PMVs released after the platelets were activated under different stimuli (Milioli et al., 2015). We compared the upstream molecules of PRKAA and the protein profiles of PMVs, and found 18 molecules in common (Fig. 4I). The 18 upstream molecules of PRKAA in PMVs are further shown in

Fig. 4J, and among them, we focused on the cAMP-dependent protein kinase (Pka) signaling pathway. Pka plays an important role in cell metabolism and phosphorylated Pka (p-Pka) has been widely reported to be an activator of phosphorylation at serine and threonine sites, and can significantly activate PRKAA at the same sites (Duca et al., 2015). Therefore, we tested the p-Pka content in microvesicles derived from collagen-activated platelets (aPMVs) or unactivated platelets (PMVs). After the concentrations of protein in the microvesicles were quantified with a BCA kit, western blotting results showed higher p-Pka levels following aPMV treatment compared with PMV treatment under the same amount of total loaded protein (Fig. 4K), which suggested an increase in the
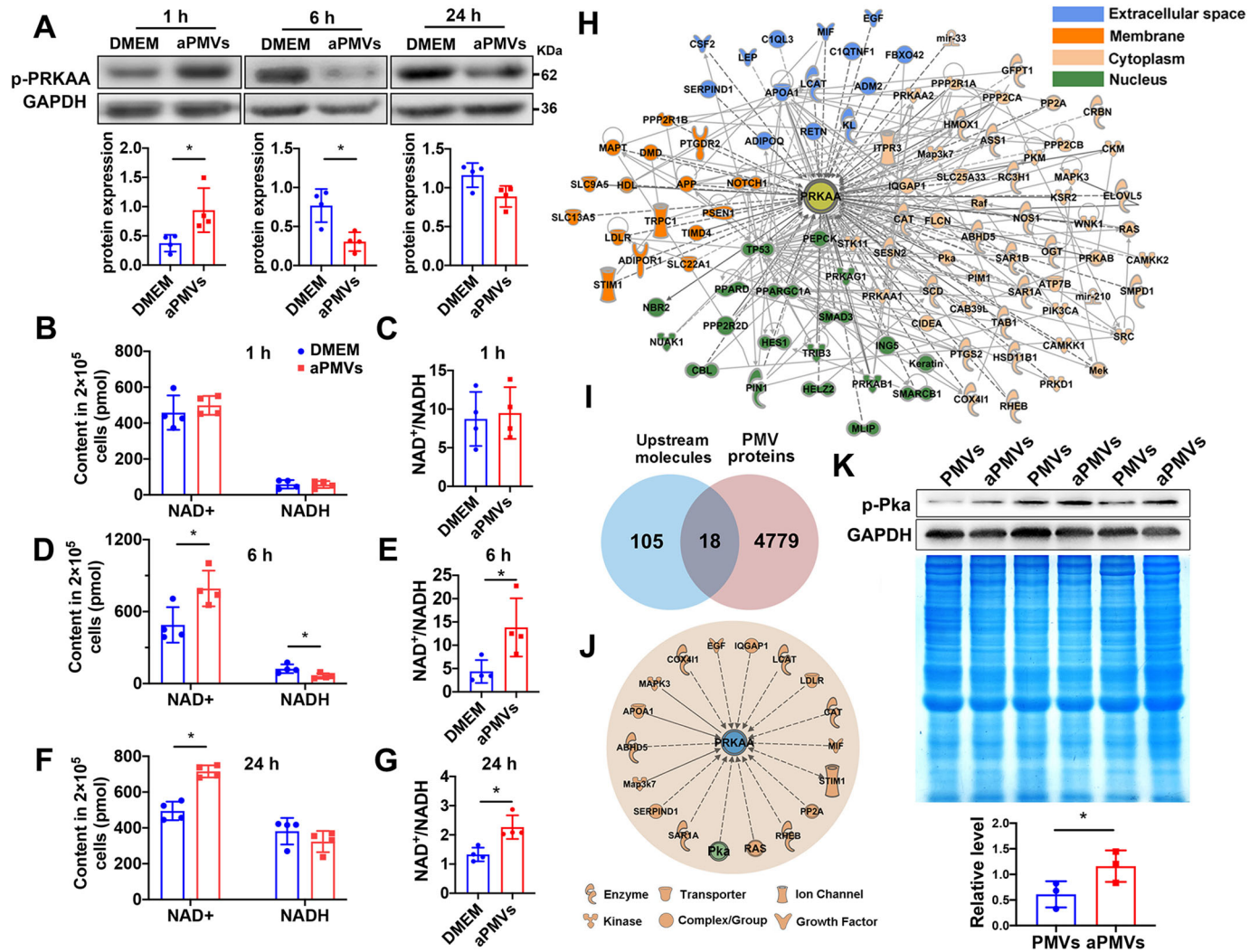
**Fig. 4. aPMV treatment modifies the protein levels of p-PRKAA and increases the NAD$^+$/NADH ratio via p-Pka.** (A) Western blot assay showed that the protein level of p-PRKAA was dramatically increased in the VSMCs after incubation with PMVs for 1 h, while the protein level decreased at 6 h and 24 h ($n=4$ independent experiments). (B,C) The contents and the ratio of NAD$^+$/NADH were not notably changed by aPMVs at 1 h ($n=4$ independent experiments). (D,E) aPMVs significantly increased the NAD$^+$ content and decreased NADH content (D) and consequently increased the NAD$^+$/NADH ratio (E) after 6 h of stimulation ($n=4$ independent experiments). (F,G) The effect of aPMVs on NAD$^+$ and NADH at 24 h was similar to the effect at 6 h ($n=4$ independent experiments). (H) The upstream molecules of PRKAA were predicted by IPA software. (I) A total of 18 molecules were predicted upstream regulators of PRKAA that were also present in the protein profile of PMVs. (J) These 18 molecules are displayed and Pka is shown in green. (K) Western blotting revealed changes in the p-Pka protein levels containing the same amount of total protein. Coomassie Blue staining was used to indicate the amount of protein that was loaded. PMVs, platelet-derived microvesicles. aPMVs, collagen activated platelet-derived microvesicles ($n=3$ independent experiments). GAPDH was used as a loading control for western blotting (A,D). *P*-values were calculated by two-tailed Mann–Whitney test (A–G,K). The values are the mean±s.d. *$P<0.05$.

secretion of p-Pka from platelets. Taken together, these data showed that collagen stimulation altered the protein levels of p-Pka contained in aPMVs, which might result in the activation of the PRKAA signaling pathway in VSMCs.

## aPMVs increase phosphorylation of FoxO1

Next, we studied the downstream molecules associated with PRKAA; 208 PRKAA downstream molecules were recognized from the IPA system, and the top ten diseases associated with these molecules are shown in Fig. 5A. Organismal injury and abnormalities are the diseases most related to the downstream molecules of PRKAA. We analyzed the direct relationship of molecules related to abnormal metabolism using the IPA database and found that both FoxO1 and FoxO3, members of the forkhead box O (FoxO) family of proteins, are at core positions (Fig. 5B). Then, we detected the mRNA expression of the FoxO proteins in

VSMCs, and found FoxO1 content to be the highest (Fig. 5C), so we focused on FoxO1 in the experiments to follow. Western blotting showed that aPMVs induced a significant increase in phosphorylated FoxO1 (p-FoxO1, Ser256) at 1 h, which persisted to 6 h. There was no significant change in protein phosphorylation at 24 h (Fig. 5D). However, FoxO1 can exert its regulatory functions through cytoplasmic and nuclear translocation after phosphorylation, so, we determined whether aPMV treatment affected the cellular localization of FoxO1 after 24 h of stimulation. Immunofluorescence results showed that p-FoxO1 gradually accumulated in the nucleus in the aPMV stimulation group in a time-dependent manner (Fig. 5E), and the relative fluorescence intensity of the nucleus gradually increased (Fig. 5F). Many studies have demonstrated the significant contribution of FoxO1 to cell proliferation and migration, and in human smooth muscle cells, FoxO1-induced gene transcription has been shown to regulate
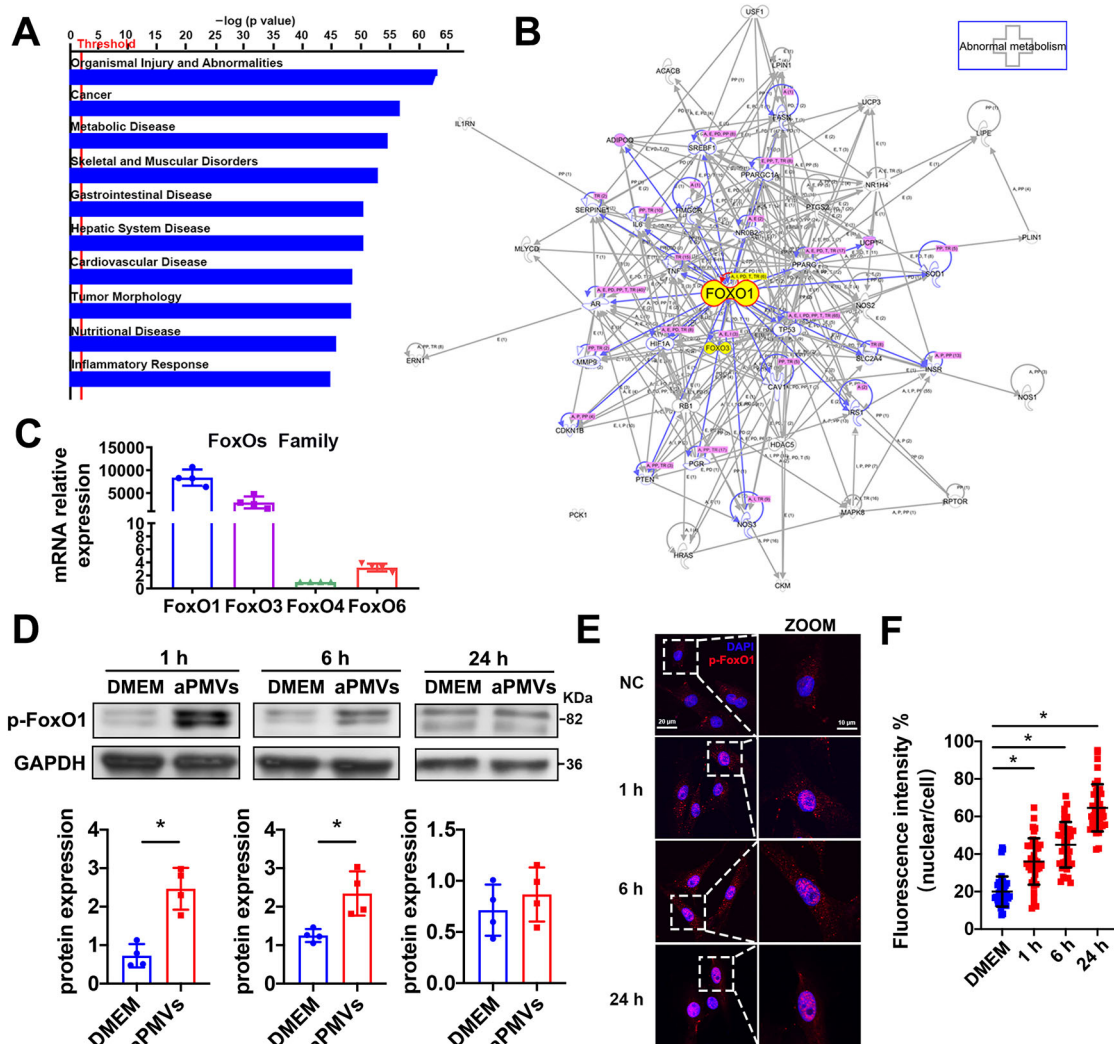
**Fig. 5. aPMV treatment increases the levels of p-FoxO1.** (A) Ingenuity pathway analysis (IPA) indicated the top ten diseases related to PRKAA downstream molecules. (B) FoxO1 and FoxO3 are at core positions of the relationship network of PRKAA downstream molecules related to abnormal metabolism. (C) mRNA levels of FoxO family proteins were analyzed using qPCR, and FoxO1 was the most abundant one ($n$=4 independent experiments). (D) Western blotting showed that after stimulation with aPMVs, the protein level of p-FoxO1 in VSMCs was significantly increased and reached its highest level at 1 h of stimulation ($n$=4 independent experiments). GAPDH was used as a loading control. (E) Immunofluorescence staining showed that aPMVs promoted the translocation of p-FoxO1 (red) from the cytoplasm to the nucleus (blue) in VSMCs. NC, negative control. Scale bars: 20 µm and 10 µm. (F) The percentage (nuclear/cell) of p-FoxO1 fluorescence intensity increased after aPMV stimulation ($n$=30 independent cells). $P$-values were calculated by two-tailed Mann–Whitney test (D) and one-way ANOVA test with Tukey's post-hoc test (F). The values are the mean±s.d. *$P$<0.05.

abnormal cell proliferation, but, more importantly, it also regulates neointimal formation (Dutzmann et al., 2021). Our results imply that p-FoxO1 might play an important role in the regulation of VSMC function.

**Compound C reverses the stimulation of VSMCs by aPMVs**
To elucidate the role of the PRKAA-NAD$^+$-FoxO1 pathway in the stimulation of VSMCs by aPMVs, we used the AMPK inhibitor Compound C (CC). First, CC significantly inhibited the protein levels of p-PRKAA, and the levels of the downstream protein p-FoxO1 then also decreased (Fig. 6A). CC also inhibited the increase in NAD$^+$/NADH 6 h after aPMV stimulation (Fig. 6B,C) but had no significant effect on the NAD$^+$/NADH ratio 24 h after stimulation (Fig. 6D,E). More interestingly, CC also affected the distribution of mitochondria in cells. Following the inhibition of PRKAA signaling, mitochondria aggregated around the nucleus in VSMCs treated with aPMVs and CC (Fig. 6F). Quantification

showed that the average distance of mitochondria from the center of the nucleus was significantly reduced (Fig. 6G,H). Based on these results, we further studied the energy metabolism in VSMCs after CC treatment.

**Compound C reverses aPMV-induced changes in VSMC energy metabolism and function**
To study the essential role of PRKAA in regulating VSMC metabolism, CC was used with aPMV treatment. We found that CC significantly reversed the effect of aPMVs on VSMC metabolism, including mitochondrial respiration (Fig. 7A) and glycolysis (Fig. 7E). CC significantly decreased the basal OCR, maximal OCR and ATP production (Fig. 7B–D) that were increased by aPMV stimulation, and upregulated the glycolysis, glycolytic capacity and glycolytic reserve (Fig. 7F–H). The presence of CC restored the energy metabolism phenotype of VSMCs (Fig. 7I). Lastly, CC significantly inhibited the migration and proliferation of
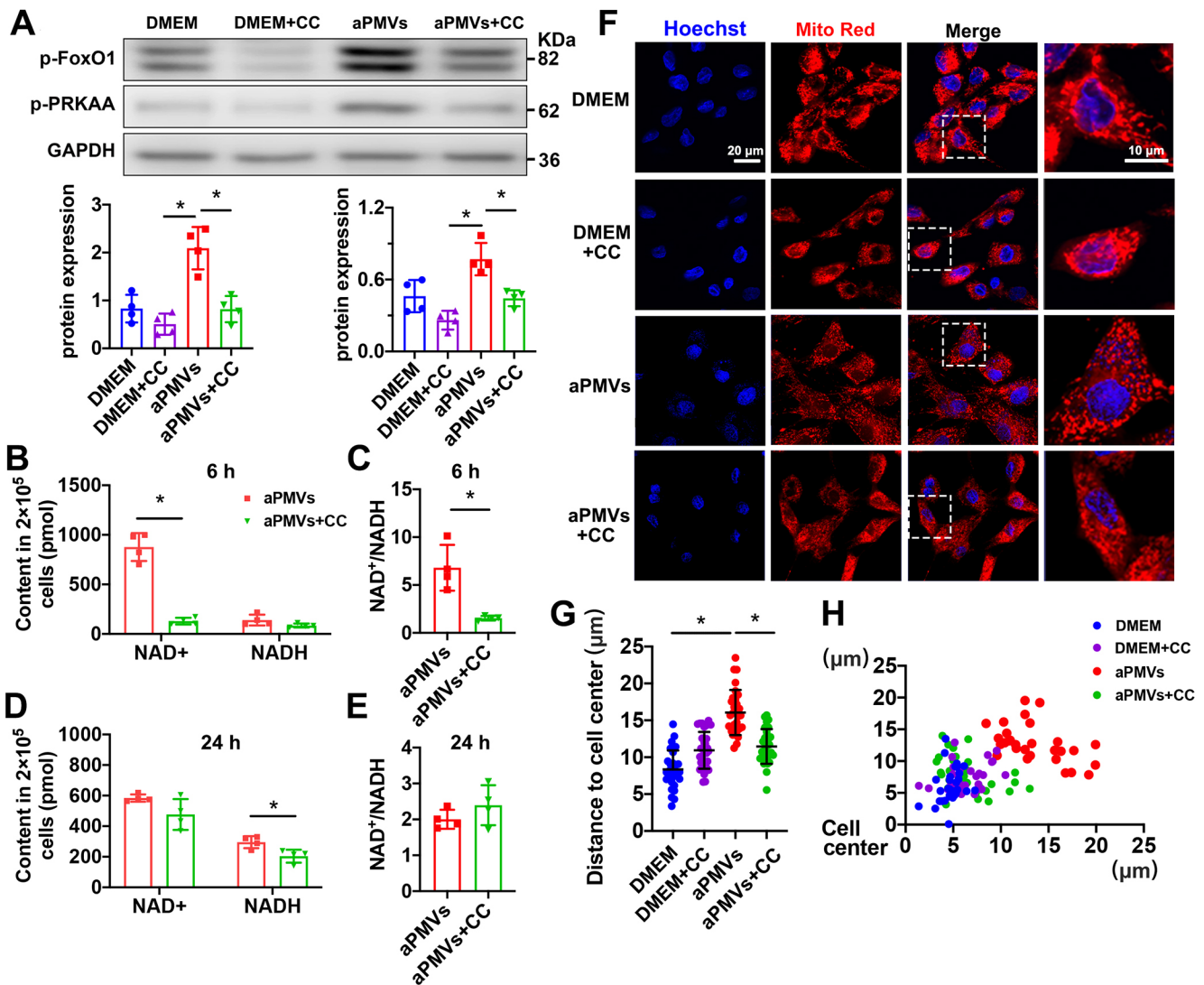
**Fig. 6. Compound C reduces p-FoxO1 levels and the NAD+/NADH ratio stimulated by aPMVs.** (A) Western blot results showed that the increased p-PRKAA and p-FoxO1 stimulated by aPMVs were downregulated with Compound C (CC) incubation (n=4 independent experiments). GAPDH was used as a loading control. (B,C) CC inhibited the NAD+ content in VSMCs and the NAD+/NADH ratio (n=4 independent experiments). (D,E) CC had no significant effect on the NAD+ content or the NAD+/NADH ratio after 24 h of stimulation with PMVs (n=4 independent experiments). (F) Effect of CC on mitochondrial distribution in VSMCs. The cells were stained with MitoTracker Red (Mito Red) and Hoechst 33342 for 30 min at 37°C. CC was incubated with VSMCs 1 h before aPMV stimulation. Scale bars: 20 µm and 10 µm. (G,H) The average distance of the mitochondria was decreased (G) and more concentrated around the nucleus after CC pretreatment (H) (n=30 independent cells). P-values were calculated by two-tailed Mann–Whitney test (B–E), Kruskal–Wallis test with uncorrected Dunn's test (A) and one-way ANOVA test with Tukey's post-hoc test (G). The values are the mean±s.d. *P<0.05.

VSMCs (Fig. 7J,K). These results showed that CC treatment significantly reversed the increased OCR and decreased the elevated ECAR, cell proliferation and migration induced by aPMV treatment. However, in the VSMCs treated with DMEM and CC, CC also had a given inhibitory effect on cell function (with significant effects on proliferation and migration only). This result might have occurred because the stimulation of aPMVs significantly activated the PRKAA pathway, which also amplifies the inhibitory effect of CC. However, in the absence of any stimulation, the cells were in a quiescent state, and the basal expression level of the PRKAA pathway and the impact on cell function were lower, so the inhibitory effect of CC was not significant. These results indicate the significant inhibitory effect of CC on signaling pathways and the critical roles of PRKAA and FoxO1 in energy metabolism, proliferation and migration.

**Compound C injection attenuated neointimal formation in vivo**

To verify the role of the PRKAA-FoxO1 pathway in VSMC migration and proliferation in vivo, we locally injected CC after rat intimal injury. The drug was administered as an injection every other day for 2 weeks at a concentration of 20 mg/kg/day. For the proliferation assay, BrdU was injected via intraperitoneal injection 24 h before sacrifice (Fig. 8A). Western blotting results indicated that p-PRKAA and p-FoxO1 were upregulated in the injured carotid arteries, which was reversed after CC treatment (Fig. 8B). Hematoxylin-Eosin (HE) staining showed that, compared with the contralateral carotid artery (control), the neointimal hyperplasia after surgery was markedly increased and was also reversed by the injection of CC (Fig. 8C). After the CC treatment, the vessel wall area was significantly reduced compared with that in the intimal injury group (Fig. 8E) without changes in the media area (Fig. 8D).
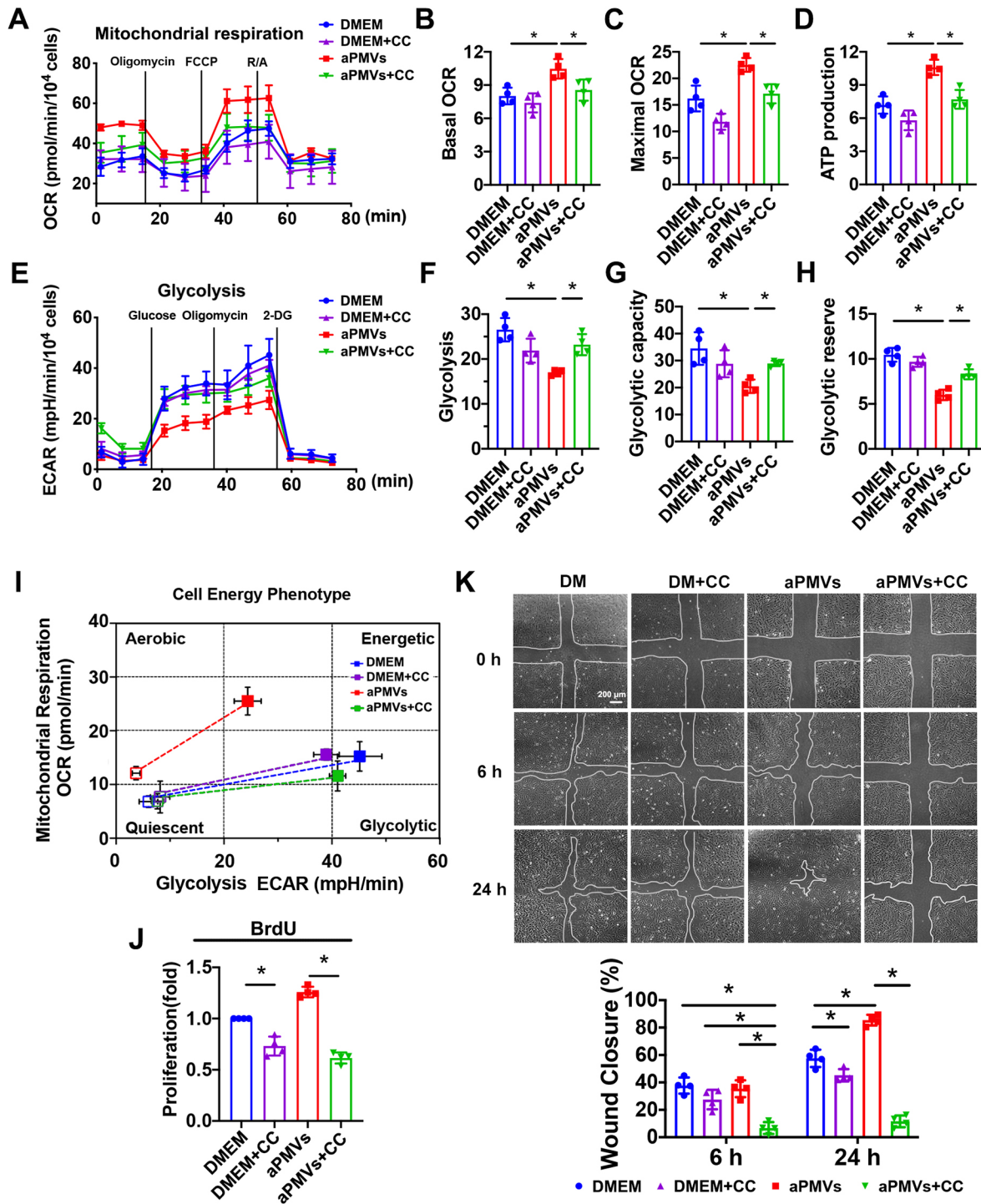
**Fig. 7. Compound C changes VSMC energy metabolism and migration stimulated by aPMVs.** (A) Representative traces of the oxygen consumption rate (OCR) in the DMEM, DMEM+CC, aPMV and aPMV+CC groups. (B) Basal OCR, (C) maximal OCR and (D) ATP production were measured and compared (A–D, n=4 independent experiments). (E) Representative traces of the extracellular acidification rate (ECAR) in the DMEM, DMEM+CC, aPMV and aPMV+CC groups. Measurement of (F) glycolysis, (G) glycolytic capacity and (H) glycolytic reserve (E–H, n=4 independent experiments). (I) Transition of the energy phenotype in VSMCs. The empty squares represent the basal cell states, and the filled squares represent the stressed cell states (n=4 independent experiments). (J,K) CC significantly inhibited the proliferation (J) and migration ability (K) of VSMCs that were increased by aPMV stimulation for 24 h (n=4 independent experiments). P-values were calculated by Kruskal–Wallis test with uncorrected Dunn's test (A–H,J,K). The values are the mean±s.d. *P<0.05.

The changes in the vascular lumen area also accounted for changes in neointimal thickness (Fig. 8F). In addition, the *in situ* proliferation assay results revealed that the number of BrdU-positive VSMCs was markedly downregulated by CC treatment (Fig. 8G–I).

The *in vivo* study results were consistent with our *in vitro* experimental results. After vascular intimal injury, VSMC migration and proliferation were increased, leading to neointimal hyperplasia. After a local injection with CC, the thickness of the
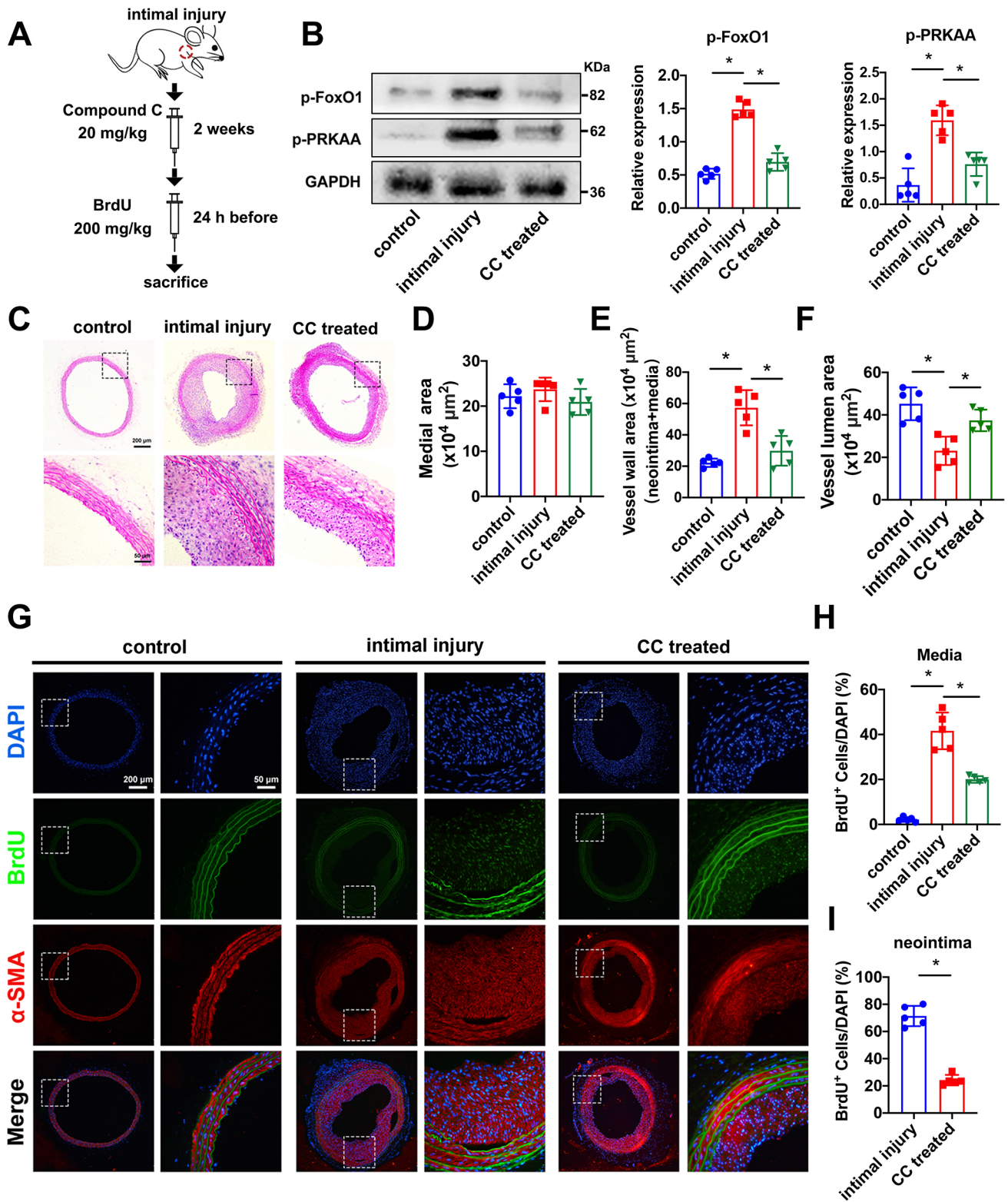
**Fig. 8. Compound C attenuates neointimal formation in intimal injury.** (A) Schematic diagram of the *in vivo* experiments. (B) Western blotting results indicated that the p-PRKAA and p-FoxO1 protein levels were upregulated after surgery and reversed by injection with CC (*n*=5 animals). GAPDH was used as a loading control. (C) Representative Hematoxylin-Eosin (HE) staining images. Scale bars: 200 µm and 50 µm. (D–F) The medial area (D), vessel wall area (E) and lumen area (F) showed that vessel neointimal hyperplasia after surgery was markedly increased and attenuated by CC treatment (C–F, *n*=5 animals). (G) Representative microscopy images revealed that VSMC proliferation in the neointima was decreased by CC injection. VSMCs were labeled with α-SMA (red), and proliferating cells showed double staining for BrdU (green) and DAPI (blue). Scale bars: 200 µm and 50 µm. (H,I) The percentage of BrdU-positive cells was downregulated by CC treatment in both the vessel area (H) and the neointima (I) (*n*=5 animals). *P*-values were calculated by Kruskal–Wallis test with uncorrected Dunn's test (B,D–F,H,I). The values are the mean±s.d. *P<0.05.

neointima was significantly reduced, thereby largely protecting the physiological function of the blood vessels.

## DISCUSSION

Here, our results demonstrated the role of aPMVs in regulating the energy metabolism and migration capacity of VSMCs via the PRKAA-NAD$^+$-FoxO1 pathway both *in vivo* and *in vitro*. Collagen-activated platelet-derived microvesicles significantly upregulated VSMC mitochondrial respiration but not glycolysis, and enhanced cell migration and proliferation. Importantly, pretreatment with the PRKAA inhibitor Compound C (CC) reversed cell function changes and the molecular signaling pathway. In addition, aPMVs delivering the upstream molecule p-Pka played a potential role in this regulation.

Intimal hyperplasia after injury has been found to serve as the basis for accelerated atherosclerosis (Motwani and Topol, 1998; Chesebro and Fuster, 1986), which is a consequence of VSMC accumulation by migration and proliferation. The mechanism underlying neointima formation has remained elusive; however, inhibiting the abnormal VSMC function seems to be a very effective way to reduce neointimal hyperplasia. For example, chicoric acid has been reported to impede VSMC proliferation, migration and neointima formation induced by platelet-derived growth factor type BB through the inhibition of the ROS-NFκB-mTOR-P70S6K pathway (Lu et al., 2018). Increased migration and proliferation of VSMCs are closely related to energy metabolism, and mitochondria play a central role in bioenergetic regulation. The subcellular localization of mitochondria is related to cellular activity, and usually more mitochondria will be distributed in the moving parts of the cell. In neurons, mitochondria travel through the microtubule network to axon terminals, fueling energy-consuming processes such as synaptic vesicle cycling (Saxton and Hollenbeck, 2012). The most intuitive finding was that the mitochondria of sperm cells were concentrated in the proximal region of the flagella and provided ATP for the motor proteins that drive sperm motility (Woolley, 1970). In our current study, we observed that aPMVs caused mitochondria to be more dispersed in cells. Cell migration is an energy-demanding process that can be fueled by dispersed mitochondria. Additionally, increased mitochondrial respiration can provide energy for VSMC proliferation.

After intima injury, the exposure of collagen components in the extracellular matrix below the endothelial layer led to platelet activation, and the activated platelets released numerous microvesicles. PMVs were first separated by ultracentrifugation in 1967 and were termed 'platelet dust' (Wolf, 1967), and were more recently reported to have a biolayer structure ranging from 100 to 1000 nm in diameter (Buzas et al., 2014). PMVs are rich in proteins, lipids and genetic information from activated platelets. Many studies have shown that PMVs have a vital effect on the development of atherosclerosis and other diseases by delivering various platelet-derived substances. PMV-derived chemokine ligand 7 (CXCL7) has been shown to contribute to glomerular endothelial injury (Zhang et al., 2018), and the resulting inflammatory cytokines increase the expression of ICAM-1 in ECs (Barry et al., 1998). Although the TEM images showed the coexistence of protein substances and extracellular vesicles in the stimulation of VSMCs, we believe that aPMVs are predominant in number. Most of these substances might be derived from platelets. For example, activated platelets release proteins through alpha granules. Using ultracentrifugation combined with density gradient centrifugation or microfiltration might improve the purity of aPMVs and reduce the influence of other proteins, which will be studied

further in our future work. In the present study, we found that compared with PMVs, aPMVs delivered higher levels of p-Pka, which could be the reason for the selective release from platelets. Pka is essential for intracellular signal transduction and the maintenance of cellular homeostatic processes. It has been widely reported to be an activator of phosphorylation at serine and threonine sites, and can significantly activate PRKAA at the same sites (Duca et al., 2015). PRKAA is a key molecule in the regulation of cellular energy metabolism, and its upstream molecule p-Pka is reportedly involved in regulating cellular energy metabolism. It has been reported that the Pka/proteasome- and Hsp90-dependent signaling pathway regulates mitochondrial respiratory chain proteins and determines cardiomyocyte energy production and functional output (Ebert et al., 2019). The study by Filteau et al. further elucidated that the extent of input signals received by Pka from various cellular processes matches its output signals, highlighting how biological processes are interconnected and coordinated by Pka because this kinase receives information from upstream and downstream processes (Filteau et al., 2015). In addition, Pka was defined as a homeostatic regulator of platelet apoptosis that determines platelet lifespan and survival (Zhao et al., 2017). After collagen activation, an increased content of p-Pka was detected in aPMVs. As an upstream regulator of PRKAA, p-Pka might play a critical role in regulating signal transduction between aPMVs and VSMCs, which we will further explore in our follow-up studies.

Studies on cellular energy metabolism, especially the relationship between glycolysis and oxidative phosphorylation have recently attracted increasing attention. VSMCs can reportedly alter their energy metabolism to meet the requirements of proliferation, which is essential for cell function maintenance and vascular pathological changes (Chiong et al., 2014). Our results indicated that aPMVs switched the VSMC energy phenotype and enhanced mitochondrial respiration. AMPK and NAD$^+$/NADH are considered critical metabolism sensors. An important role for AMPK has been proposed, and the balance between NAD$^+$ synthesis and consumption supports fundamental mitochondrial functions, including oxidative phosphorylation and the tricarboxylic acid cycle (Klimova et al., 2020). The hydrogen from intermediate products in the metabolic process is given to NAD$^+$ to form reduced NADH, which supplies reducing equivalents to the mitochondrial electron transport chain (ETC) to fuel oxidative phosphorylation. Earlier reports have demonstrated that NAD$^+$/NADH plays a decisive role in hyperglycemia-induced VSMC migration and proliferation (Yasunari et al., 1997). The regulatory effect of AMPK on NAD$^+$ has also been reported. The AMPK-NAD$^+$-SIRT1 signaling pathway has been tightly linked to mitochondrial function (Price et al., 2012), and has been extensively studied in aging as well (Nacarelli et al., 2019). Cantó et al. (2009) showed that AMPK enhances SIRT1 activity by increasing cellular NAD$^+$ levels, resulting in the modulation of the activity of downstream SIRT1 targets that include the transcription factors FoxO1 and FoxO3a. Our IPA results revealed the regulatory relationship between AMPK-NAD$^+$ and FoxO, so we further explored the changes in FoxO family proteins and found that FoxO1 was activated by aPMVs.

FoxO proteins are an important class of redox-sensitive transcription factors that includes four members: FoxO1/FKHR, FoxO3/FKHRL1, FoxO4/AFX and FoxO6 (Kim et al., 2018). FoxO1 is a newly discovered regulator of energy metabolism that corrects the imbalance of energy metabolism in the body. Calvier et al. (2017) identified a pro-proliferative TGFβ1-Stat3-FoxO1 pathway in VSMCs that properly regulated energy metabolism and

cell proliferation. Mindin, an extracellular matrix component, has been reported to cause metabolic disorders by inhibiting abnormal VSMC migration, proliferation and phenotypic switching in a FoxO1-dependent manner (Zhu et al., 2015). Phosphorylated FoxO1 can enter the nucleus and combine with DNA, which can be altered by acetylation (Matsuzaki et al., 2005), to regulate downstream target genes and VSMC phenotypic transformation (Deng et al., 2015). Previous studies have shown that VSMCs with a synthetic phenotype trigger the development of vascular diseases (Miano et al., 2021), and this phenotype promotes VSMC proliferation and migration (Wang et al., 2021), resulting in vascular intima thickening. In the current study, we also explored whether the phenotype of VSMCs was regulated by aPMVs, and the decreases in the VSMC markers, calponin, α-SMA and SM22α, indicated that VSMCs switch from a contractile phenotype to a synthetic phenotype (Fig. S3). A study focusing on the role of p-FoxO1 in VSMC energy metabolism and phenotypic transformation will be conducted to provide more evidence for the mechanism of vascular neointimal hyperplasia.

In conclusion, we first observed the effect of aPMVs on VSMC energy metabolism and explored the underlying molecular mechanism. Our results provide new insight into the process by which aPMVs regulate the energy metabolism and migration of VSMCs via the PRKAA-FoxO1 pathway after intimal injury (Fig. S4). After PRKAA is inhibited by CC, the level of phosphorylated FoxO1 and the NAD$^+$/NADH ratio decrease, leading to the reversal of the VSMC energy metabolic profile and eventually inhibiting excessive cell migration. Our results reveal a potential therapeutic target for inhibiting the neointimal hyperplasia of injured intima.

## MATERIALS AND METHODS
### Establishment of a rat carotid artery intimal injury model
Animal care and handling complied with the policies of the Animal Management Rules (File 55, 2001, Ministry of Health, China). The experiment was approved by the Animal Research Committee of Shanghai Jiao Tong University, and conformed to the guidelines from the US NIH Guide for the Care and Use of Laboratory Animals.

Sprague-Dawley (SD) rats (350–400 g) were anesthetized by inhalation of isoflurane (induction 4%, maintenance 2%, in 2 liters/min O$_2$). After the carotid artery was exposed using narrow instruments, the occipital artery, internal carotid artery, thyroid artery and external carotid artery were ligated in sequence. In the intimal injury experiment, a 2.0 Fogarty balloon (Edwards Lifesciences, Irvine, CA, USA) with an inflatable balloon at the tip of the hollow guide wire was used. It was inserted into the common external carotid artery through a small incision on the external carotid artery, and inflation caused the balloon to expand and fill the entire blood vessel. While the balloon was kept expanded, it was slowly withdrawn from the vessel, causing uniform damage to the intima. After that, the balloon was restored to the contracted state and inserted into the blood vessel again, repeating the above steps three times. Carotid arteries were harvested at 1 h and 2 weeks after the surgery.

For the Compound C (CC) local injection, the operated rats were anesthetized with isoflurane. After CC was dissolved in normal saline, the drug was injected intramuscularly in the surgical side of the rat's neck using a 1 ml sterile syringe. The technician avoided plunging the needle too deeply during injection to avoid puncturing the vessel. The first injection was 3 h after surgery, and then the drug was injected every other day for 2 weeks.

### Collection of platelet-derived microvesicles
Differential centrifugation was used for microvesicle isolation. Whole blood was collected from the abdominal aortas of anesthetized rats into syringes with 100 μl/ml anticoagulant [2.94% sodium citrate, 136 mM glucose (pH 6.4)], and transferred to 5 ml normal saline containing 5 mM EDTA,

0.1 g/ml prostaglandin E1 (PGE1) and 1 U/ml apyrase. Then, platelet-rich plasma was obtained by centrifugation at 600 $g$ for 15 min. Platelets were prepared from platelet-rich plasma by centrifugation at 2000 $g$ for 15 min and resuspended in the same volume of whole blood with modified Tyrode solution [12 mM NaHCO$_3$, 138 mM NaCl, 5.5 mM glucose, 2.9 mM KCl, 2 mM MgCl$_2$, 0.42 mM NaH$_2$PO$_4$ and 10 mM 4-(2-hydroxyethyl)-1-piperazineethanesulfonic acid (pH 7.4)]. Platelets were activated with collagen (1 μl/ml) in a 37°C water bath for 1 h, and the platelets that had not been activated with collagen were placed in the same water bath. After the platelets were collected, the remaining platelet-poor plasma was centrifuged at 20,500 $g$ for 90 min to obtain collagen-activated platelet microvesicles (aPMVs) and untreated platelet-derived microvesicles (PMVs). The collected microvesicles were suspended in Dulbecco's Modified Eagle Medium (DMEM) for further cell stimulation at a concentration of 10$^9$ microvesicles/ml or suspended in normal saline for further testing.

### Isolation and cultivation of VSMCs
VSMCs were collected from the freshly isolated thoracic aortas of SD rats using an explanted technique (Richard et al., 2012; Qi et al., 2016). First, the thoracic aortas were surgically isolated and transferred to a cell culture dish and washed with PBS containing penicillin (100 U/ml) and streptomycin (0.1 mg/ml). Then, the aortas were minced into small pieces after the adventitia were peeled off and the remaining tissue was digested with collagenase I to remove the endothelium. The small pieces were plated onto a cell culture dish containing DMEM (Gibco, Grand Island, NY, USA) with 10% newborn calf serum (NBCS; Gibco, Grand Island, NY, USA) and incubated at 37°C in an incubator with 5% CO$_2$. The VSMC monolayers were passaged every 2–3 days after trypsinization, and the cells in passages 4–7 were used for experiments. In the *in vitro* experiment, VSMCs were seeded at a density of 2.0×10$^5$ cells per well in six-well plates. VSMCs incubated with aPMVs/PMVs for 1, 6 or 24 h at 37°C with 5% CO$_2$ were used as the experimental groups (aPMVs/PMVs), and cells treated with DMEM were used as the control groups (DMEM). VSMCs were treated with 10 μm Compound C (CC; Selleck Chemicals, Houston, TX, USA) for 1 h before stimulation.

### Identification of platelet-derived microvesicles
Nanoparticle tracking analysis (NTA) (Szatanek et al., 2017) was used to confirm the size and concentration of the PMVs. The collected PMVs were resuspended in PBS, and an isopycnic suspension for each group was injected into the NanoSight apparatus (NanoSight NS300; Malvern Panalytical, London, UK) for assessment.

Transmission electron microscopy (TEM; Talos L120C G2, Thermo Fisher Scientific, Waltham, MA, USA) was used to visualize the vesicles. A small amount of the microvesicle suspension was dropped on the hydrophilic TEM grid, dried, washed three times with double-distilled water and stained with phosphotungstic acid for 1 min.

Flow cytometry (Cytoflex; Beckman Coulter Co. Ltd, Indianapolis, IN, USA) was used to identify the collected microvesicles. FITC-labeled CD63 (1:100; ab108949; Abcam, Cambridge, UK) was used as a marker of exosomes, Annexin A1 (1:100; 55018-1-AP; Proteintech, Chicago, IL, USA) stained with APC secondary antibody (1:1000; ab130805; Abcam, Cambridge, UK) was used as a marker of microvesicles, and CD41 (1:100; ab181582; Abcam, Cambridge, UK) stained with Alexa Fluor 488 secondary antibody (1:1000; 4412S; Cell Signaling Technology, Danvers, MA, USA) was used as a marker of platelets. The samples were incubated with primary antibodies for 2 h at 4°C, and with secondary antibodies for 1 h at room temperature.

### Adhesion of aPMVs to VSMCs
To confirm the adhesion of aPMVs to VSMCs, aPMVs were incubated with PKH26, a fluorescent dye that stains living cells (PKH26 Fluorescent Cell Linker Kits; Millipore Sigma, Billerica, MA, USA). We used a DiO live cell membrane green fluorescent probe (Beyotime Biotechnology, Shanghai, China) to label the cell membrane in accordance with the manufacturer's instructions. Fluorescent labeling of the two colors was performed separately and the samples were washed after staining to ensure that there was no unbound staining. VSMCs were washed with PBS to remove serum

in confocal dishes, and a DiO green fluorescent probe was added to the DMEM at a concentration of 1:200. Cells were stained for 10 min and then gently washed with PBS twice to remove the green probe. aPMVs were resuspended in 100 µl serum-free DMEM and PKH26 was added at a concentration of 1:1000 labeling for 10 min. Then, 900 µl of DMEM with 10% NBCS was added to stop the labeling reaction according to the manufacturer's instructions. After that, the aPMVs were centrifuged at 20,500 *g* to remove the PKH26 and were resuspended in DMEM with 10% NBCS. PKH26-aPMVs (in red) and DiO-VSMCs (in green) were co-incubated for 0 h, 1 h, 6 h or 24 h. Nuclei were marked in blue with Hoechst 33342 (Beyotime Biotechnology). All the groups were washed with PBS before detection. The images were ultimately captured using confocal microscopy (LV1000; Olympus Corporation, Shinjuku-ku, Tokyo, Japan).

### Immunofluorescence staining and Hematoxylin-Eosin staining

VSMCs were fixed in 4% paraformaldehyde for 20 min and then permeabilized in 0.3% Triton X-100 for 3 min. After being washed with PBS, the VSMCs were immersed in 10% goat serum at room temperature for 30 min and incubated with primary antibodies against p-FoxO1 at a concentration of 1:100 (Cell Signaling Technology, Danvers, MA, USA) at 4°C overnight. On the second day, the VSMCs were incubated with the secondary antibody (1:1000, Cell Signaling Technology) at room temperature for 2 h after being washed with PBS. DAPI was then used to stain the cell nuclei for 15 min at room temperature. The freshly isolated carotid arteries were immediately placed in 4% paraformaldehyde, incubated for 24 h and dehydrated in 30% sucrose solution at 4°C. These carotid arteries were cut into frozen sections with a thickness of 8 µm and used for immunofluorescence (IF). For IF, the sections were incubated with primary antibodies against CD41 (1:200, ab181582, Abcam, Cambridge, UK), vWF (1:200, Bs-10048R, Bioss, Beijing, China) or α-SMA (1:200, F3777, Sigma, Billerica, MA, USA). Images were captured by confocal microscopy.

Hematoxylin-Eosin (HE) staining was used to observe vascular morphology. The carotid arteries were fixed with 10% formaldehyde in PBS for 24 h and dehydrated with increasing concentrations of ethanol (30%, 50%, 75%, 85%, 95% and 100%). After incubation with a mixture of xylene and anhydrous ethanol (1:1), xylene I and xylene II, the arteries were dipped into melted paraffin, and the embedded arteries were cut into sections with a thickness of 8 µm. During the next steps, xylene I, xylene II and decreasing concentrations of ethanol were sequentially used for dewaxing and hydrating. After being stained with hematoxylin for 3 min, the sections were rinsed with distilled water, and immersed in 0.1% hydrochloric acid in ethanol for 5 s. After being rinsed with tap water, the sections were treated with Reverse Blue solution (Beyotime Biotechnology, Shanghai, China) for 5 min and stained with Eosin for 1 min. Increasing concentrations of ethanol were used for dehydration, followed by xylene, xylene I and xylene II. Images were captured by microscopy (Olympus, BX51) and the vascular lumen area and thickness were analyzed with ImageJ.

### Quantitative real-time PCR

The total RNA from each sample was isolated with TRIzol Reagent. Then, 1 ml of TRIzol was added to each well of six-well plates containing VSMCs, and the total RNA was transferred into RNA enzyme-free tubes. The collected total RNA was extracted with chloroform, and then treated with isopropanol and 75% ethanol for collection. After the optical density (OD) was measured, reverse transcription (RT) was performed. The reverse transcription system was: 3 µg of RNA, 1 µl of Oligo-dT primer and RNase-free water (made up to 12 µl), which were incubated at 65°C for 5 min; then, 4 µl of 5× Reaction Buffer, 2 µl of 10 mM dNTP, 1 µl reverse transcriptase and 1 µl RNase inhibitor were added to each sample to reach a total volume of 20 µl, and the samples were then incubated at 42°C for 1 h and 70°C for 5 min. cDNA was stored at −80°C or used for quantitative real-time PCR (qPCR). The qPCR system was as follows: 10 µl of SYBR Green Supermix (TaKaRa, Kyoto, Japan), 0.4 µl of forward primer, 0.4 µl of reverse primer, 3 µl of cDNA and 6.2 µl of RNase-free water and the total volume was made up to 20 µl. The PCR conditions were 95°C for 5 min, followed by 40 cycles

at 95°C for 5 s, 60°C for 45 s and 72°C for 30 s using a StepOnePlus real-time PCR system (Applied Biosystem, Foster City, CA, USA). The results were eventually normalized to the level of GAPDH mRNA, and the expression of different genes was measured by the $2^{-\Delta\Delta CT}$ method. The primer information is provided in Table S1.

### Western blot assay

The total protein from the cells was collected with loading buffer and then boiled for 5 min. Proteins were separated by 10% SDS-PAGE and electrophoretically transferred to PVDF membranes. The membranes were blocked with 5% non-fat milk at room temperature for 1 h. After being washed with Tris-buffered saline with Tween-20 (TBST) three times, the membranes were incubated overnight with primary antibodies against p-PRKAA (1:1000; 2535T, Cell Signaling Technology, Danvers, MA, USA), p-FoxO1 (1:1000; 9461, Cell Signaling Technology, Danvers, MA, USA) and GAPDH (1:1000; 60004-1-lg, Proteintech, Chicago, IL, USA) at 4°C. The second day, the membranes were incubated with horseradish peroxidase-conjugated antibodies (1:1000; 7076S, Cell Signaling Technology, Danvers, MA, USA) at room temperature for 2 h after being washed with TBST three times. An extreme hypersensitivity ECL chemiluminescence kit (BeyoECl Moon; Beyotime Biotechnology, Shanghai, China) was used to develop the blots. The final grayscale signals of the target protein were captured with the Fusion Fx Imaging System (VILBER LOURMAT, Paris, France) and quantified with Image Studio. All antibody information is provided in Table S2. A BCA kit (Beyotime Biotechnology, Shanghai, China) was used to quantify the protein levels. Original data for western blots is shown in Fig. S5.

### Wound healing assay

VSMCs were seeded into six-well plates and cultured to 90% confluence. A cross line was drawn in the monolayer of VSMCs at the same position in each well to cause wounds, and the cells were washed with PBS. The wound area was determined using ImageJ software at different time points (0 h, 6 h or 24 h), and images were taken with microscope. Then the wound closure percentage was determined by: $\left(1 - \dfrac{\text{wound area}(6\,\text{h or }24\,\text{h})}{\text{wound area}(0\,\text{h})}\right) \times 100\%$. Five random fields were captured for observation and statistics.

### Proliferation assay

The proliferation of VSMCs *in vitro* was determined by using BrdU cell proliferation ELISA kit (Fluos; Roche, Basel, Switzerland). In brief, BrdU labeling reagent was added to the culture medium (1:1000) 8 h before detection. Then, VSMCs were fixed and incubated with antibody (1:100) according to the manufacturer's instructions. The absorbance was measured over a wavelength range of 450–630 nm.

The *in vivo* VSMC proliferation assay was analyzed using the *In Situ* Cell Proliferation Kit (Roche). 24 h before vessel harvest, BrdU was intraperitoneally injected into the rats at a concentration of 200 mg/kg. Arteries were fixed and dehydrated in isopentane for 24 h, and then frozen sections with a thickness of 10 µm were produced and stored at −20°C. The frozen sections were re-softened in PBS, fixed with 70% ethanol in 50 mM glycine buffer, digested with 0.05% trypsin solution and denatured with 2 M HCl. The samples were incubated with anti-BrdU antibody (1:200, from the kit) overnight. The nuclei were stained with DAPI the next day. Blood vessels were dissected longitudinally and flattened between coverslips. Fluorescence microscopy (Olympus, BX51) was used to visualize BrdU-positive cells.

### NAD⁺/NADH assay

Both the $NAD^+$ and NADH levels were determined using an $NAD^+$/NADH quantification kit (Beyotime Biotechnology, Shanghai, China). The assay is based on using WST-8 to detect the amount and ratio of $NAD^+$ and NADH in cells by colorimetry. The absorbance was measured at 450 nm and was proportional to the $NAD^+$ and NADH concentration in the sample.

### Metabolic function evaluation

To measure cellular mitochondrial respiration and glycolysis simultaneously, the Seahorse XF Cell Mito Stress Test Kit and Glycolysis Stress Test Kit were used (Agilent Technologies, Delaware, USA) by

following the manufacturer's instructions using a Seahorse XF96 Flux Analyzer (Agilent Technologies, Delaware, USA).

In brief, VSMCs were seeded in an XF96 cell culture microplate ($1 \times 10^4$ cells per well). Oligomycin (1.5 μM), FCCP (1 μM), and Rotenone/ Antimycin A (R/A) (0.5 μM) were injected sequentially to measure the oxygen consumption rate (OCR). Rotenone is an inhibitor of complex I (NADH dehydrogenase complex), and Antimycin A is an inhibitor of complex III (cytochrome b/c1 complex). The combined effect of the two substances can shut down cellular respiration by inhibiting the mitochondrial electron transport chain. After this treatment, the non-mitochondrial respiration driven by the process outside the mitochondria can be calculated. To measure the extracellular acidification rate (ECAR), D-glucose (10 mM), oligomycin (1 μM) and 2-deoxy-D-glucose (2-DG; 50 mM) were injected sequentially into a cell culture microplate. The OCR and ECAR data were normalized to the actual cell number. After the Seahorse analysis completed, the cells were washed with PBS and stained with DAPI for cell counting. Then the High-Content Analysis System (Operetta CLS, Waltham, MA, USA) was applied to count the cell number.

### Mitochondrial distribution analysis

To observe the distribution of mitochondria in VSMCs, cells were stained with MitoTracker Red (Beyotime Biotechnology, Shanghai, China) at 37°C for 30 min, and nuclei were stained with DAPI diluted in PBS (1:1000). Cells were randomly selected, and photos were captured by confocal microscopy (LV1000, Olympus). The quantification of the mitochondrial distribution was performed using CellSens Dimension software (Olympus Corporation, Shinjuku-ku, Tokyo, Japan).

### Ingenuity pathway analysis

IPA software (Qiagen, Dusseldorf, Germany) was used to search for molecules related to PRKAA through the Grow Tool. After the prediction, the possible functional classifications and canonical pathways of the target molecules were obtained. The significance values for analyses were calculated using the right-tailed Fisher's exact test.

### Statistical analysis

The '*n*' in the experiments refers to biological repetitions, and all the values are displayed as the mean±s.d. For data comparisons on less than 30 (<30) samples, nonparametric tests were used. Two-tailed Mann–Whitney test was used for the comparison between two samples. For multiple comparisons, the Kruskal–Wallis test with uncorrected Dunn's test was used. For experiments with a sample size of greater than 30 (>30), the Shapiro–Wilk test was first performed for the normality test, and then the unpaired two-tailed Student's *t*-test and one-way ANOVA test with Tukey's post-hoc test were used for the comparison between two samples and multiple comparisons among the groups, respectively. GraphPad Prism 8 software was used for graphing and statistical analysis. $P < 0.05$ was considered statistically significant.

### Author contributions

Methodology: J.Y., Y.-J.F., H.B., S.-M.Z.; Investigation: Y.-G.L., Q.-P.Y.; Resources: Y.-L.H., Z.-L.J., Y.-X.Q.; Writing - review & editing: J.Y., Y.H.; Supervision: Y.H.; Project administration: Y.H.; Funding acquisition: Y.H.

### Peer review history

The peer review history is available online at https://journals.biologists.com/jcs/ article-lookup/doi/10.1242/jcs.259364.

## References

**Barry, O. P., Praticò, D., Savani, R. C. and FitzGerald, G. A.** (1998). Modulation of monocyte-endothelial cell interactions by platelet microparticles. *J. Clin. Invest.* **102**, 136-144. doi:10.1172/JCI2592

**Boilard, E., Nigrovic, P. A., Larabee, K., Watts, G. F. M., Coblyn, J. S., Weinblatt, M. E., Massarotti, E. M., Remold-O'Donnell, E., Farndale, R. W., Ware, J. et al.** (2010). Platelets amplify inflammation in arthritis via collagen-dependent microparticle production. *Science* **327**, 580-583. doi:10.1126/science. 1181928

**Buzas, E. I., György, B., Nagy, G., Falus, A. and Gay, S.** (2014). Emerging role of extracellular vesicles in inflammatory diseases. *Nat. Rev. Rheumatol.* **10**, 356-364. doi:10.1038/nrrheum.2014.19

**Calvier, L., Chouvarine, P., Legchenko, E., Hoffmann, N., Geldner, J., Borchert, P., Jonigk, D., Mozes, M. M. and Hansmann, G.** (2017). PPARγ Links BMP2 and TGFb1 pathways in vascular smooth muscle cells, regulating cell proliferation and glucose metabolism. *Cell Metab.* **25**, 1118-1134. doi:10.1016/ j.cmet.2017.03.011

**Cantó, C., Gerhart-Hines, Z., Feige, J. N., Lagouge, M., Noriega, L., Milne, J. C., Elliott, P. J., Puigserver, P. and Auwerx, J.** (2009). AMPK regulates energy expenditure by modulating NAD+ metabolism and SIRT1 activity. *Nature* **458**, 1056-1060. doi:10.1038/nature07813

**Carracedo, M., Artiach, G., Arnardottir, H. and Bäck, M.** (2019). The resolution of inflammation through omega-3 fatty acids in atherosclerosis, intimal hyperplasia, and vascular calcification. *Semin. Immunopathol.* **41**, 757-766. doi:10.1007/ s00281-019-00767-y

**Cheong, A., Li, J., Sukumar, P., Kumar, B., Zeng, F., Riches, K., Munsch, C., Wood, I. C., Porter, K. E. and Beech, D. J.** (2011). Potent suppression of vascular smooth muscle cell migration and human neointimal hyperplasia by KV1.3 channel blockers. *Cardiovasc. Res.* **89**, 282-289. doi:10.1093/cvr/cvq305

**Chesebro, J. H. and Fuster, V.** (1986). Platelet-inhibitor drugs before and after coronary artery bypass surgery and coronary angioplasty: the basis of their use, data from animal studies, clinical trial data, and current recommendations. *Cardiology* **73**, 292-305. doi:10.1159/000174022

**Chiong, M., Cartes-Saavedra, B., Norambuena-Soto, I., Mondaca-Ruff, D., Morales, P. E., Garcia-Miguel, M. and Mellado, R.** (2014). Mitochondrial metabolism and the control of vascular smooth muscle cell proliferation. *Front. Cell Dev. Biol.* **2**, 72. doi:10.3389/fcell.2014.00072

**Deng, L., Huang, L., Sun, Y., Heath, J. M., Wu, H. and Chen, Y.** (2015). Inhibition of FOXO1/3 promotes vascular calcification. *Arterioscler. Thromb. Vasc. Biol.* **35**, 175-183. doi:10.1161/ATVBAHA.114.304786

**Duca, F. A., Côté, C. D., Rasmussen, B. A., Zadeh-Tahmasebi, M., Rutter, G. A., Filippi, B. M. and Lam, T. K. T.** (2015). Metformin activates a duodenal Ampk-dependent pathway to lower hepatic glucose production in rats. *Nat. Med.* **21**, 506-511. doi:10.1038/nm.3787

**Dutzmann, J., Haertlé, M., Daniel, J.-M., Kloss, F., Musmann, R.-J., Kalies, K., Knöpp, K., Pilowski, C., Sirisko, M., Sieweke, J.-T. et al.** (2021). BET bromodomain-containing epigenetic reader proteins regulate vascular smooth muscle cell proliferation and neointima formation. *Cardiovasc. Res.* **117**, 850-862. doi:10.1093/cvr/cvaa121

**Ebert, A., Joshi, A. U., Andorf, S., Dai, Y., Sampathkumar, S., Chen, H., Li, Y., Garg, P., Toischer, K., Hasenfuss, G. et al.** (2019). Proteasome-dependent regulation of distinct metabolic states during long-term culture of human iPSC-derived cardiomyocytes. *Circ. Res.* **125**, 90-103. doi:10.1161/CIRCRESAHA. 118.313973

**Faubert, B., Vincent, E. E., Poffenberger, M. C. and Jones, R. G.** (2015). The AMP-activated protein kinase (AMPK) and cancer: many faces of a metabolic regulator. *Cancer Lett.* **356**, 165-170. doi:10.1016/j.canlet.2014.01.018

**Filteau, M., Diss, G., Torres-Quiroz, F., Dubé, A. K., Schraffl, A., Bachmann, V. A., Gagnon-Arsenault, I., Chrétien, A. È., Steunou, A.-L., Dionne, U. et al.** (2015). Systematic identification of signal integration by protein kinase A. *Proc. Natl. Acad. Sci. USA* **112**, 4501-4506. doi:10.1073/pnas. 1409938112

**Jeppesen, D. K., Fenix, A. M., Franklin, J. L., Higginbotham, J. N., Zhang, Q., Zimmerman, L. J., Liebler, D. C., Ping, J., Liu, Q., Evans, R. et al.** (2019). Reassessment of exosome composition. *Cell* **177**, 428-445.e18. doi:10.1016/ j.cell.2019.02.029

**Kim, C. G., Lee, H., Gupta, N., Ramachandran, S., Kaushik, I., Srivastava, S., Kim, S.-H. and Srivastava, S. K.** (2018). Role of Forkhead Box Class O proteins in cancer progression and metastasis. *Semin. Cancer Biol.* **50**, 142-151. doi:10.1016/j.semcancer.2017.07.007

**Klimova, N., Fearnow, A., Long, A. and Kristian, T.** (2020). NAD+ precursor modulates post-ischemic mitochondrial fragmentation and reactive oxygen species generation via SIRT3 dependent mechanisms. *Exp. Neurol.* **325**, 113144. doi:10.1016/j.expneurol.2019.113144

**Lu, Q.-B., Wan, M.-Y., Wang, P.-Y., Zhang, C.-X., Xu, D.-Y., Liao, X. and Sun, H.-J.** (2018). Chicoric acid prevents PDGF-BB-induced VSMC dedifferentiation, proliferation and migration by suppressing ROS/NFκB/mTOR/P70S6K signaling cascade. *Redox. Biol.* **14**, 656-668. doi:10.1016/j.redox.2017.11.012

**Mathieu, M., Névo, N., Jouve, M., Valenzuela, J. I., Maurin, M., Verweij, F. J., Palmulli, R., Lankar, D., Dingli, F., Loew, D. et al.** (2021). Specificities of

exosome versus small ectosome secretion revealed by live intracellular tracking of CD63 and CD9. *Nat. Commun.* **12**, 4389. doi:10.1038/s41467-021-24384-2

**Matsuzaki, H., Daitoku, H., Hatta, M., Aoyama, H., Yoshimochi, K. and Fukamizu, A.** (2005). Acetylation of Foxo1 alters its DNA-binding ability and sensitivity to phosphorylation. *Proc. Natl. Acad. Sci. USA* **102**, 11278-11283. doi:10.1073/pnas.0502738102

**Merlet, E., Atassi, F., Motiani, R. K., Mougenot, N., Jacquet, A., Nadaud, S., Capiod, T., Trebak, M., Lompré, A.-M. and Marchand, A.** (2013). miR-424/322 regulates vascular smooth muscle cell phenotype and neointimal formation in the rat. *Cardiovasc. Res.* **98**, 458-468. doi:10.1093/cvr/cvt045

**Miano, J. M., Fisher, E. A. and Majesky, M. W.** (2021). Fate and state of vascular smooth muscle cells in atherosclerosis. *Circulation* **143**, 2110-2116. doi:10.1161/CIRCULATIONAHA.120.049922

**Milioli, M., Ibáñez-Vea, M., Sidoli, S., Palmisano, G., Careri, M. and Larsen, M. R.** (2015). Quantitative proteomics analysis of platelet-derived microparticles reveals distinct protein signatures when stimulated by different physiological agonists. *J. Proteomics* **121**, 56-66. doi:10.1016/j.jprot.2015.03.013

**Mishra, P. and Chan, D. C.** (2016). Metabolic regulation of mitochondrial dynamics. *J. Cell Biol.* **212**, 379-387. doi:10.1083/jcb.201511036

**Motwani, J. G. and Topol, E. J.** (1998). Aortocoronary saphenous vein graft disease: pathogenesis, predisposition, and prevention. *Circulation* **97**, 916-931. doi:10.1161/01.CIR.97.9.916

**Nacarelli, T., Lau, L., Fukumoto, T., Zundell, J., Fatkhutdinov, N., Wu, S., Aird, K. M., Iwasaki, O., Kossenkov, A. V., Schultz, D. et al.** (2019). NAD+ metabolism governs the proinflammatory senescence-associated secretome. *Nat. Cell Biol.* **21**, 397-407. doi:10.1038/s41556-019-0287-4

**Osman, I. and Segar, L.** (2016). Pioglitazone, a PPARγ agonist, attenuates PDGF-induced vascular smooth muscle cell proliferation through AMPK-dependent and AMPK-independent inhibition of mTOR/p70S6K and ERK signaling. *Biochem. Pharmacol.* **101**, 54-70. doi:10.1016/j.bcp.2015.11.026

**Perez, J., Hill, B. G., Benavides, G. A., Dranka, B. P. and Darley-Usmar, V. M.** (2010). Role of cellular bioenergetics in smooth muscle cell proliferation induced by platelet-derived growth factor. *Biochem. J.* **428**, 255-267. doi:10.1042/BJ20100090

**Price, N. L., Gomes, A. P., Ling, A. J. Y., Duarte, F. V., Martin-Montalvo, A., North, B. J., Agarwal, B., Ye, L., Ramadori, G., Teodoro, J. S. et al.** (2012). SIRT1 is required for AMPK activation and the beneficial effects of resveratrol on mitochondrial function. *Cell Metab.* **15**, 675-690. doi:10.1016/j.cmet.2012.04.003

**Qi, Y.-X., Yao, Q.-P., Huang, K., Shi, Q., Zhang, P., Wang, G.-L., Han, Y., Bao, H., Wang, L., Li, H.-P. et al.** (2016). Nuclear envelope proteins modulate proliferation of vascular smooth muscle cells during cyclic stretch application. *Proc. Natl. Acad. Sci. USA* **113**, 5293-5298. doi:10.1073/pnas.1604569113

**Richard, P. M., Jan, L. P. and Emily, W.** (2012). Vascular smooth muscle cells: isolation, culture, and characterization. *Methods Mol. Biol.* **843**, 169-176. doi:10.1007/978-1-61779-523-7_16

**Rigoulet, M., Bouchez, C. L., Paumard, P., Ransac, S., Cuvellier, S., Duvezin-Caubet, S., Mazat, J. P. and Devin, A.** (2020). Cell energy metabolism: an update. *Biochim. Biophys. Acta Bioenerg.* **1861**, 148276. doi:10.1016/j.bbabio.2020.148276

**Rosińska, J., Łukasik, M. and Kozubski, W.** (2017). The impact of vascular disease treatment on platelet-derived microvesicles. *Cardiovasc. Drugs Ther.* **31**, 627-644. doi:10.1007/s10557-017-6757-7

**Salabei, J. K. and Hill, B. G.** (2013). Mitochondrial fission induced by platelet-derived growth factor regulates vascular smooth muscle cell bioenergetics and cell proliferation. *Redox Biol.* **1**, 542-551. doi:10.1016/j.redox.2013.10.011

**Saxton, W. M. and Hollenbeck, P. J.** (2012). The axonal transport of mitochondria. *J. Cell Sci.* **125**, 2095-2104. doi:10.1242/jcs.053850

**Seifert, J., Rheinlaender, J., Lang, F., Gawaz, M. and Schäffer, T. E.** (2017). Thrombin-induced cytoskeleton dynamics in spread human platelets observed with fast scanning ion conductance microscopy. *Sci. Rep.* **7**, 4810. doi:10.1038/s41598-017-04999-6

**Sinnetta, S. E. and Brenman, J. E.** (2014). Past strategies and future directions for identifying AMP Activated Protein Kinase (AMPK) modulators. *Pharmacol. Ther.* **143**, 111-118. doi:10.1016/j.pharmthera.2014.02.008

**Szatanek, R., Baj-Krzyworzeka, M., Zimoch, J., Lekka, M., Siedlar, M. and Baran, J.** (2017). The methods of choice for extracellular vesicles (EVs) characterization. *Int. J. Mol. Sci.* **18**, 1153. doi:10.3390/ijms18061153

**Tesfamariam, B.** (2016). Endothelial repair and regeneration following intimal injury. *J. Cardiovasc. Transl. Res.* **9**, 91-101. doi:10.1007/s12265-016-9677-1

**Théry, C., Witwer, K. W., Aikawa, E., Alcaraz, M. J., Anderson, J. D., Andriantsitohaina, R., Antoniou, A., Arab, T., Archer, F., Atkin-Smith, G. K. et al.** (2018). Minimal information for studies of extracellular vesicles 2018 (MISEV2018): a position statement of the International Society for Extracellular Vesicles and update of the MISEV2014 guidelines. *J. Extracell. Vesicles.* **23**, 1535750. doi:10.1080/20013078.2018.1535750

**Wanet, A., Arnould, T., Najimi, M. and Renard, P.** (2015). Connecting mitochondria, metabolism, and stem cell fate. *Stem Cells Dev.* **24**, 1957-1971. doi:10.1089/scd.2015.0117

**Wang, F., Zhen, Y., Si, C., Wang, C., Pan, L., Chen, Y., Liu, X., Kong, J., Nie, Q., Sun, M. et al.** (2021). WNT5B promotes vascular smooth muscle cell dedifferentiation via mitochondrial dynamics regulation in chronic thromboembolic pulmonary hypertension. *J. Cell. Physiol.* **237**, 789-803. doi:10.1002/jcp.30543

**Wolf, P.** (1967). The nature and significance of platelet products in human plasma. *Br. J. Haematol.* **13**, 269-288. doi:10.1111/j.1365-2141.1967.tb08741.x

**Woolley, D. M.** (1970). The midpiece of the mouse spermatozoon: its form and development as seen by surface replication. *J. Cell Sci.* **6**, 865-879. doi:10.1242/jcs.6.3.865

**Yasunari, K., Kohno, M., Kano, H., Yokokawa, K., Minami, M. and Yoshikawa, J.** (1997). Mechanisms of action of troglitazone in the prevention of high glucose-induced migration and proliferation of cultured coronary smooth muscle cells. *Circ. Res.* **81**, 953-962. doi:10.1161/01.RES.81.6.953

**Zeng, M. L., He, Y., Du, H. X., Yang, J. H. and Wan, H. T.** (2020). Output regulation and function optimization of mitochondria in eukaryotes. *Front. Cell Dev. Biol.* **8**, 598112. doi:10.3389/fcell.2020.598112

**Zhang, Y., Ma, K. L., Gong, Y. X., Wang, G. H., Hu, Z. B., Liu, L., Lu, J., Chen, P. P., Lu, C. C., Ruan, X. Z. et al.** (2018). Platelet microparticles mediate glomerular endothelial injury in early diabetic nephropathy. *J. Am. Soc. Nephrol.* **29**, 2671-2695. doi:10.1681/ASN.2018040368

**Zhang, W.-X., Tai, G.-J., Li, X.-X. and Xu, M.** (2019). Inhibition of neointima hyperplasia by the combined therapy of linagliptin and metformin via AMPK/Nox4 signaling in diabetic rats. *Free Radic. Biol. Med.* **143**, 153-163. doi:10.1016/j.freeradbiomed.2019.07.030

**Zhao, L., Liu, J., He, C., Yan, R., Zhou, K., Cui, Q., Meng, X., Li, X., Zhang, Y., Nie, Y. et al.** (2017). Protein kinase A determines platelet life span and survival by regulating apoptosis. *J. Clin. Invest.* **127**, 4338-4351. doi:10.1172/JCI95109

**Zhu, L.-H., Huang, L., Zhang, X. J., Zhang, P., Zhang, S.-M., Guan, H. J., Zhang, Y., Zhu, X.-Y., Tian, S., Deng, K. Q. et al.** (2015). Mindin regulates vascular smooth muscle cell phenotype and prevents neointima formation. *Clin. Sci. (Lond.)* **129**, 129-145. doi:10.1042/CS20140679

**Zhuang, T., Liu, J., Chen, X. L., Pi, J. J., Kuang, Y. S., Wang, Y. F., Tomlinson, B., Chan, P., Zhang, Q., Li, Y. et al.** (2019). Cell-specific effects of GATA (GATA Zinc Finger Transcription Factor Family)-6 in vascular smooth muscle and endothelial cells on vascular injury neointimal formation. *Arterioscler. Thromb. Vasc. Biol.* **39**, 888-901. doi:10.1161/ATVBAHA.118.312263